Chemical Engineering Communications

ISSN: 0098-6445 (Print) 1563-5201 (Online) Journal homepage: https://www.tandfonline.com/loi/gcec20

TiO_2/ZnO Supported on Sepiolite: Preparation, Structural Characterization, and Photocatalytic Degradation of Flumequine Antibiotic in Aqueous Solution

Ali İmran Vaizoğullar

To cite this article: Ali İmran Vaizoğullar (2017) TiO_2/ZnO Supported on Sepiolite: Preparation, Structural Characterization, and Photocatalytic Degradation of Flumequine Antibiotic in Aqueous Solution, Chemical Engineering Communications, 204:6, 689-697, DOI: 10.1080/00986445.2017.1306518

To link to this article: https://doi.org/10.1080/00986445.2017.1306518

Chemical Engineering Communications, 204:689–697, 2017

ISSN: 0098-6445 print/1563-5201 online
DOI: 10.1080/00986445.2017.1306518

TiO_2/ZnO Supported on Sepiolite: Preparation, Structural Characterization, and Photocatalytic Degradation of Flumequine Antibiotic in Aqueous Solution

ALI İMRAN VAIZOĞULLAR

Vocational School of Health Care, Medical Laboratory Program, Muğla Sıtkı Koçman University, Muğla, Turkey

In this study, TiO_2, ZnO, TiO_2/ZnO (Ti/Zn), and TiO_2/ZnO/Sep (Ti/Zn/Sep) catalysts have been synthesized using sol–gel and chemical precipitation method. Their photocatalytic performances have been compared using Flumequine (FLQ) antibiotic. X-ray diffraction (XRD), Fourier transform infrared spectra (FTIR), scanning electron microscopy (SEM), N_2-adsorption, and the determination of a zero point charge has been used to characterize the synthesized catalysts. The degradation studies showed that the catalytic efficiency of Ti/Zn/Sep is higher than that for other catalysts. The operational parameters such as pH, initial FLQ concentration, and catalyst dosage were evaluated. UV–vis and high-resolution mass spectroscopy (HRMS) analyses were used to determine the degradation efficiency and products. ZnO played a major role in the FLQ degradation process, and sepiolite contributed to adsorption of FLQ on the catalyst surface enormously. The catalysts exhibited 11%, 23%, 63%, and 85% degradation efficiency for ZnO, TiO_2, Ti/Zn, and Ti/Zn/Sep in the decomposition of FLQ, respectively.

Keywords: Clay/TiO_2; Flumequine; Sepiolite; TiO_2/ZnO; TiO_2/ZnO/Sep

Introduction

Recently, pharmaceutical compounds such as antibiotics have been observed in surface water, ground water, sewage effluent, and drinking water (Elmolla and Chaudhuri, 2010). These compounds can come from hospital waste, human excretion, or the pharmaceutical industry (Nikolaou et al., 2007). Several researchers have expressed the belief that antibiotics such as norfloxacin affect the environment negatively. Also, they can cause allergies and toxicity and can lead to the formation of antibiotic-resistant bacteria (Chen and Chu, 2012; Palominos et al., 2008). Flumequine (FLQ) is widely used in fish farms due to it being a broad-spectrum antibiotic. "Due to its continuous introduction into the environment and resistance to degradation, FLQ residues have been detected in aquatic environments (2.5–50 ng/L) and in soil (6.9 µg/g)" (Rodrigues-Silva et al., 2013). To solve and protect such environmental issues and human health, an advanced oxidation process has been used as an effective treatment technique when compared with others such as activated carbon adsorption and reverse osmosis (Wang et al., 2015). During the oxidation process, semiconductor materials such as TiO_2 have been used as the most efficient catalyst for the photocatalytic degradation process under UV light (Hadjltaief et al., 2016). Also, many researchers have expressed that composite TiO_2, such as TiO_2/ZnO, TiO_2/ZrO_2, TiO_2/CeO_2, and SiO_2/TiO_2 are the better catalyst than pure TiO_2 for the removal of organic pollutants (Zhou et al., 2008). The synthesis of these metal oxides is an important detail in industrial applications, but some problems may occur in practice. To overcome these problems, metal oxides can be modified with the introduction of inert materials.

Clay minerals have been widely used for the removal of toxic materials from water, and it is likely to be an optimal alternative material for study (Abollino et al., 2008; Bhattacharyya and Gupta, 2008). Uğurlu and Karaoğlu (2011) put forward the idea that clay-assisted metal oxides have more enhanced photoactivity than bare metal oxide. Sepiolite is a potential carrier because of its alkali and acidic center. This structure created the adsorbed molecules on the sepiolite surface easily became an activated compound, which results in increased and more efficient degradation (Xu et al., 2010).

In this study, TiO_2/ZnO was immobilized on a natural sepiolite clay surface using the sol–gel method. Catalysts were characterized by Fourier transform infrared spectra (FTIR), scanning electron microscopy (SEM), and X-ray diffraction (XRD) advanced analytical techniques. Surface properties were evaluated using Brunauer–Emmett–Teller (BET) results. The photocatalytic performance of TiO_2, ZnO, and TiO_2/ZnO/Sep was observed for the removal of the FLQ antibiotic under UV light. Solution pH, catalyst dosage, and the initial FLQ concentration were selected as operational parameters. Our focus in this

Address correspondence to Ali İmran Vaizoğullar, Vocational School of Health Care, Medical Laboratory Program, Muğla Sıtkı Koçman University, 48700, Muğla, Turkey. E-mail: aliimran@mu.edu.tr

Color versions of one or more of the figures in the article can be found online at www.tandfonline.com/gcec.

paper is in a comparative study by synthesizing a new catalyst. Its degradation yield and the most efficient degradation conditions were investigated.

Materials and Methods

Preparation of TiO_2, ZnO, TiO_2/ZnO, TiO_2/ZnO/Sep

TiO_2 was prepared using the sol–gel method using titanium tetra butoxide (TBT, Sigma-Aldrich, 97%). About 5 ml of TBT and 25 ml of absolute ethanol (C_2H_5OH, Merck) was mixed with 50 ml of deionized water. The mixed solution was then stirred for 4 h, after which the solution was separated by centrifugation; the particles were washed several times with distilled water and ethanol before drying at 80°C for 4 h and calcined at 500°C for 3 h.

ZnO particles were synthesized using a chemical precipitation method. For this, 2 g of zinc acetate ($Zn(Ac)_2$, Merck) was dissolved in an ethanol–water (10/40) mixture and then 0.1 M of potassium hydroxide (KOH, Merck) was added drop by drop to this solution. It was stirred for 6 h at room temperature, after which it was dried and calcined at 400°C for 2 h. Ti/Zn nanoparticles were synthesized using the sol–gel method. Then, 5 ml of TBT (reagent grade 97%) and 2 g of $Zn(Ac)_2 \cdot 6H_2O$ containing 15 ml of C_2H_5OH and 100 ml of $H_2O/N(C_2H_5OH)_3$ mixture (including 20 ml $N(C_2H_5OH)_3$) were stirred at 60°C for 2 h. The obtained particles were filtered and washed with distilled water and dried at 90°C then calcined at 600°C for 3 h.

TiO_2/ZnO/Sep particles were synthesized as the same Ti/Zn catalyst, the only difference being adding 5 g of raw sepiolite (Sep) to the solution and prepared in the same conditions.

Characterizations

The crystalline phase was examined by XRD (Rigaku Dmax 350) using copper K radiation ($\lambda = 0.154056$ nm). The IR analysis of the catalyst was carried out using the Thermo-Scientific IR measurement system (Nicolet IS10-ATR). The microstructure and shape of the particle were investigated using SEM (JEOL JSM-7600F) instrument. The elemental composition was determined using a (JEOL JSM-7600F) EDAX analyzer with a SEM measurement. The BET, pore volume, and pore size were measured using ASAP 2010 (Micromeritics Instrument Corporation, USA) with N_2 adsorption at 77.35 K. UV-DRS analyses were performed between 200 and 800 nm using a Shimadzu 1601 UV–vis spectrophotometer. The isoelectric point (IEP) of catalyst was determined by a zeta sizer using electrophoretic light scattering method (Nano S, Malvern Instruments). High-resolution mass spectroscopy (HRMS) analysis was performed by a Waters SYNAPT G1 MS system (ESI-TOF-MS) between 50 and 300 Da with capillary voltage 3.5 kV, sampling cone 30 V, extraction cone 4 V, source temperature 80°C, and desolvation temperature 250°C, and was performed using an ESI ionization technique on a Q-TOF mass spectrometer.

The crystallite size of all the catalysts was calculated using the Scherer equation:

$$d = \frac{B\lambda}{\beta_{1/2}\cos\theta} \quad (1)$$

Table I. Physiochemical properties of catalyst

Catalyst	BET (m^2/g)	Pore size (nm)	Pore volume (cm^3/g)	Langmuir surface area (m^2/g)	Crystal size (nm)
TiO_2	10.02	11.99	0.0301	17.01	22.3
ZnO	1.56	8.83	0.0034	2.27	78.9
Ti/Zn	51.31	10.84	0.139	63.21	29.2
Ti/Zn/Sep	118.28	13.85	0.4092	158.27	17.8
Sepiolite	305.08	7.17	0.5756	392.22	–

where d is the average particle size, B is the Scherer constant (0.91), λ is the wavelength of the X-ray, $\beta_{1/2}$ is full width at half maximum (FWHM) of the diffraction peak, and θ is the diffraction angle. The surface physical properties of the prepared catalyst, including pore volume, surface area, and surface morphology were examined and the results are summarized in Table I.

Photocatalytic Experiments

In photolytic experiments, a specially designed UV reactor was used. This reactor consists of a closed system having a Spectroline XX-15 N UV lamp which emits radiation at 260 nm with the intensity of 2 mW/cm^2 together with properties allowing fixed mixing and cooling and oxygen entry. An FLQ solution (10 mg/L) was freshly prepared and 50 ml of portions and 0.2 g of the catalyst were transferred into the UV reactor and stirred for 60 min in the dark to obtain adsorption/desorption equilibrium. After degradation had begun, 1 ml of the sample was withdrawn and filtered every 60 min to determine the degradation rates. Then the absorbance of the supernatant was determined using a Dr. Lange spectrophotometer. The spectrophotometric measurements at the maximum wavelength (248 nm) were used to find the degradation rate of the FLQ. The degradation percentage of the FLQ was calculated using the following equation:

$$\%\text{Degradation} = \frac{C_{o-}C}{C_o} \times 100 \quad (2)$$

where C_0 is the initial concentration of FLQ, and C is FLQ concentration at any time. To explain the photocatalytic reaction mechanisms of the catalyst under UV light, 1 mM of different radical scavengers (isopropyl alcohol (IPA), potassium iodide (KI), and ascorbic acid (AA)) were added to the photocatalytic reaction system. The photocatalytic reaction of these oxidative species is the same as photocatalytic degradation experiments. In addition to the experiments, an attempt to identify of FLQ decomposition intermediates HRMS analysis was performed.

Results and Discussion

FTIR Analysis

To identify each catalyst, the FTIR results were evaluated. From the FTIR spectrum of ZnO (Figure 1(a)), the broad peak at 3430 cm^{-1} is the stretching vibrating peaks of the O–H bond in the surfaced hydroxyl in ZnO (Figure 1(a)) (Wang et al.,

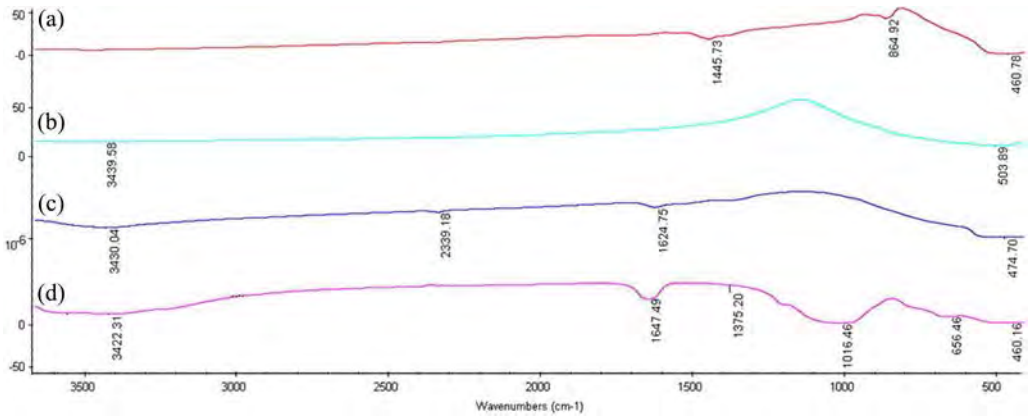

Fig. 1. FTIR spectra of ZnO (a), TiO_2 (b), Ti/Zn (c), and TiO_2/ZnO/Sep (d) catalysts.

2014). From Figure 1(b), the band at 503 cm^{-1} indicates the stretching mode of metal oxide bonds in TiO_2 (Gnanaprakasam et al., 2015). The band observed at 1620 cm^{-1} is attributed to the stretching vibrations of the Zn–O bonds. The peak at 474 cm^{-1} is the characteristic absorption peak of the Zn–O (Figure 1(c)). These results confirm the Zn–O bonds (Singh et al., 2012). The band at 2339 cm^{-1} can be attributed to by-products which occurred in the reaction medium (Figure 1(c)). In Figure 1(d), it can be clearly seen that the bands at 3572 and 3422 cm^{-1} can be attributed to the O–H stretching of the water on the catalyst surface. The peaks at 1647 and 460 cm^{-1} belong to the Zn–O stretching modes (Figure 1(d)). The Si–O and O–H bands can be clearly observed in the FTIR spectra of TiO_2/ZnO/Sep. The band at 1016 cm^{-1} is the Si–O stretching group of the tetrahedral sheet. Therefore, these peaks could be used to authenticate the sepiolite clay. The band at 656 cm^{-1} is the deformation vibration of Mg_3OH groups (Madejov and Komadel, 2001).

SEM and EDAX Analysis

To explain their morphologies of the catalysts, SEM and EDAX analyses were carried out for all catalysts. Figure 2 shows the SEM image of the TiO_2, ZnO, Ti/Zn, and Ti/Zn/Sep nanoparticles.

From the SEM images shown in Figure 2, it can be seen that all particles are an irregular shape. The morphology of Ti/Zn particles contains two different structures first rods-like ZnO and nearly spherical TiO_2 (Figure 2(c)). Two different structures confirm the combination of TiO_2 and ZnO particles defined as

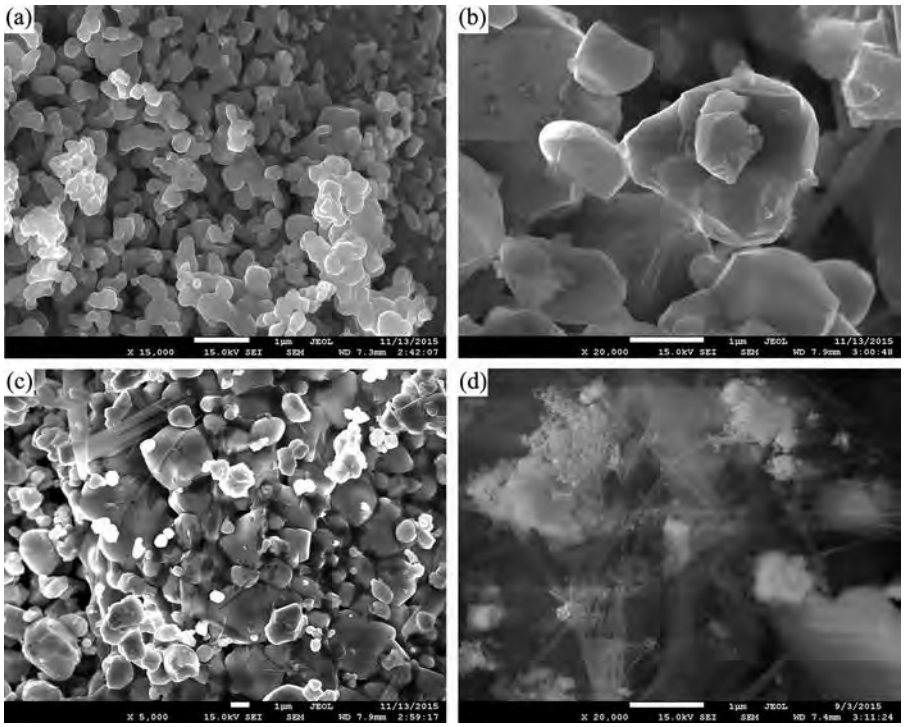

Fig. 2. SEM images of TiO_2 (a), ZnO (b), Ti/Zn (c), and Ti/Zn/Sep (d).

Ti/Zn. As shown in Figure 2(d), SEM image of sepiolite clay shows a fibrous morphology. The particle size of Ti/Zn/Sep is not entirely apparent due to agglomeration (Figure 2(d)). TiO_2 and ZnO are seen as aggregated on sepiolite structure. Because of its smaller particle size, the surface energy of Ti/Zn/Sep increased. This is because of agglomeration of particles (Gnanaprakasam et al., 2015).

XRD Analysis

Figure 3 represents the XRD pattern of TiO_2 (a), ZnO (b), Ti/Zn (c), and Ti/Zn/Sep (d) catalysts, respectively. The sharp peaks which belong to TiO_2 and ZnO indicate that the catalysts were finely crystallized (Figures 3(a) and (b)). Figure 3(a) shows the appearance of peaks at $2\theta = 25.28°$, 37.75°, 48.5°, 55.13°, and 62.71°, corresponding to the anatase phase of TiO_2 (Mahdavi et al., 2013). The absolute rutile peak at ~27.4° was not observed. This result implies that all peaks are anatase form of TiO_2. The peaks at $2\theta = 31.77°$, 34.46°, 36.29°, 47.57°, 56.62° 62.89°, 68.11°, and 69.11° have been attributed to the hexagonal wurtzite phase of ZnO (JPDS 36-1451) (Figure 3(b)). As shown in Figure 3(c), anatase form of TiO_2 and Wurtzite phases of ZnO were observed in the XRD pattern. This indicates the combination of anatase TiO_2 and wurtzite ZnO composites. From Figure 3(c), it can be seen that the diffraction peak intensities of anatase decreased with the addition of ZnO, it is likely because the highly dispersed ZnO particles may shelter the TiO_2 surface from the emitted XRD (Li et al., 2015). It is also important to note that no another unassigned peak appears in these XRD patterns. This fact apparently means that no other zinc or titanium phases crystallized during the synthesis. From Figure 3(d), the phase percentages of anatase and rutile were obtained from the formula $A(\%) = 100/1 + 1.265\ \{I_R|I_A\}$, using integrated intensity of the anatase and rutile phases (Hadjltaief et al., 2016). Where I_A and I_R are the intensity of the anatase and the rutile phases at 25.38° and 27.48° 2θ, respectively. The calculated phase percentage of anatase and rutile are 89% and 11% in Ti/Zn/Sep catalyst, respectively.

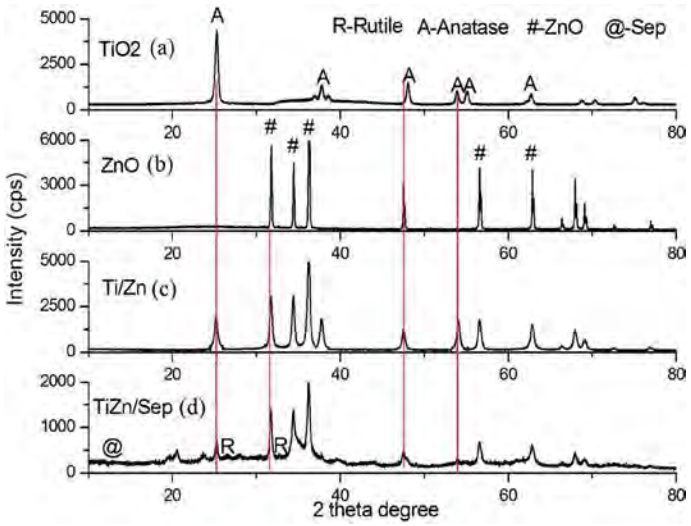

Fig. 3. XRD spectrum of TiO_2, ZnO, Ti/Zn, and Ti/Zn/Sep.

These results are likely to be related to calcination temperature during the calcination process. The size of synthesized particles was calculated using Equation (1). The peak intensity and FWHM values were determined from the XRD analysis. The FWHM value, which was located in the Debye–Scherer formula, is derived from the strongest peak for the catalysts. The average crystalline sizes of TiO_2, ZnO, Ti/Zn, and Ti/Zn/Sep catalysts were found to be 22.5, 78.9, 29.2, and 17.8 nm, respectively (Table I).

The textural properties of the catalysts are given in Table I. It is clear that the BET surface area of Ti/Zn/Sep catalyst is higher than that of the ZnO, TiO_2, and Ti/Zn catalysts. Also, the BET surface area of the Ti/Zn/Sep catalyst is found to be 118.28 m^2/g, which is less than fibrous sepiolite. The reduction in the surface area of Ti/Zn/Sep is attributed to the considerable absorption of TiO_2 and ZnO particles on the sepiolite surface. The crystalline size of particles also shows that sepiolite acted as both supported material and size-controlling material.

Operational Parameters

Effect of pH

The influence of pH was conducted ranging from 2 to 10 using HCl (0.1 M) and NaOH (0.1 M). FLQ concentration was taken to be 10 mg/L for 0.1 g/50 ml of the Ti/Zn/Sep catalyst. The results of the effect of pH are shown in Figure 4(a). It can be seen from Figure 4 that the decomposition of FLQ increased with increase in the pH and then decreased. This result can be explained by IEP of Ti/Zn/Sep catalyst. The zeta potential measurement of the Ti/Zn/Sep catalyst is shown in Figure 4(b). As predicted, the IEP of Ti/Zn/Sep is about 6.8. The surface of Ti/Zn/Sep is positive below at IEP, in contrast, is negative above at IEP. Electrostatic attraction between Ti/Zn/Sep and FLQ can cause an increase in adsorption and degradation efficiently. These results can be explained by the fact that the surface charge of the Ti/Zn/Sep catalyst was positive which decreased the attraction between the Ti/Zn/Sep and FLQ ($pK_a = 6.32$) molecules at a low pH value; however, both catalyst and FLQ surfaces negatively charge which increased repulsion at a high pH value. Therefore at the optimum pH value, the affinity between the catalyst and the FLQ was optimal, causing higher photocatalytic activity (Palominos et al., 2008).

Catalyst Dosage and Initial Concentration

The catalyst concentration in the photocatalytic system plays an important role and catalyst is directly proportional to the overall catalytic reaction rate (Eydivand and Nikazar, 2015). In this study, a series of experiments was carried out by varying the amount of the catalyst in the range of 0.1–1 g. Figure 5 shows the effect of catalyst concentration on the degradation of the FLQ. It can be clearly seen that the greatest degradation was found at 0.2 g of catalyst dosage and the degradation removal rate achieved by 72%. At a higher than 0.2 g catalyst dosage, the degradation rates significantly decreased. This can be explained through the fact that when the number of the catalyst

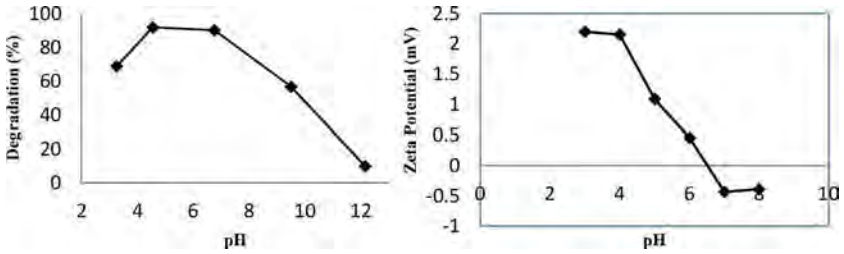

Fig. 4. Effect of pH and zeta potential measurement of Ti/Zn/Sep catalyst.

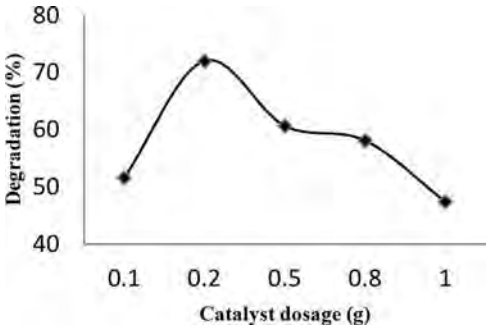

Fig. 5. The effect of catalyst dosage for degradation of FLQ using Ti/Zn/Sep catalyst ($FLQ_o = 10$ mg/L, 50 ml volume of solution and pH of IEP).

molecules increases because of lower photon absorption, the light scattering occurs during the reaction resulting in a reduction in light penetration through the solution (Zhu et al., 2000). This result confirms the association between the penetration of light and active sites of the catalyst. Thus, for practical reasons, 0.2 g was chosen as the optimum catalyst dosage (Figure 5).

Some researchers have expressed that to obtain efficient degradation, highly concentrated solutions can be diluted (Robert and Malato, 2002), in contrast very low concentrations exhibit low adsorption rate. Therefore, in this study, the initial concentration rate was investigated. For this, the initial concentration of FLQ varied from 1 to 20 mg/L at a fixed IEP. From Figure 6, when the concentration of the FLQ was increased from 1 to 10 mg/L, the degradation percentage increased and then decreased. The maximum degradation efficiency was achieved for 71% within 240 min when the initial FLQ concentration was 10 mg/L. This can be explained as due to excess of FLQ molecules in the medium caused steric hindrance and Van der Wall repulsion, therefore the percentage removal decreased after the 10 mg/L of FLQ concentration.

Kinetic Isotherm and Photocatalytic Studies

The data shown in Figure 7 were used to calculate the apparent rate constants (k_{app}) for different catalyst samples. The pseudo-first-order equation can be used to explain the kinetics of the photocatalytic degradation of FLQ. The first-order kinetic rate k (1/min) for FLQ degradation can be calculated by plotting $\ln \frac{C_0}{C}$ versus time (t). The experimental conditions are as follows: pH = 5, 0.2 g of catalyst dosage, 10 mg/L of initial FLQ concentration, and 240 min of reaction time. The k_{app} values increase in the sequence of the photolysis as: ZnO, TiO_2, Ti/Zn, and Ti/Zn/Sep. The regression coefficient (R^2) value of Ti/Zn/Sep catalyst is very close to 0.98 (Ye et al., 2015). This indicated that the data agreed with the pseudo-first-order isotherm for the Ti/Zn/Sep catalyst as shown in Figure 8. The correlation constant for the lines was calculated to be $R^2 = 0.97$. The kinetic results revealed that Ti/Zn/Sep catalyst has the highest photoactive compared with the others. It has highly degraded the FLQ in a period of 240 min (Table II).

Direct photolysis of FLQ shows insignificant results, and the photocatalytic degradation of FLQ by TiO_2, ZnO, and Ti/Zn under UV irradiation exhibit 23%, 11%, and 67% degradation efficiency, respectively (Figure 7). Without adding sepiolite, Ti/Zn composite shows more catalytic activity than bare TiO_2 and ZnO catalysts. This can be attributed to the synergetic effect of

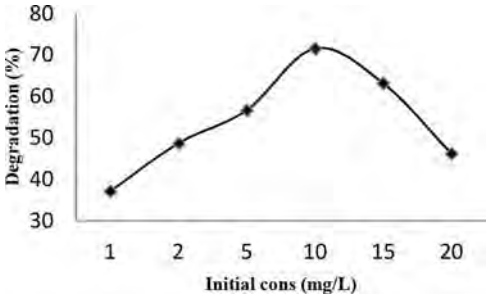

Fig. 6. Effect of initial FLQ concentration on the photocatalytic degradation of FLQ (catalyst dosage 0.1 g, 50 ml volume of FLQ solution, and pH of IEP).

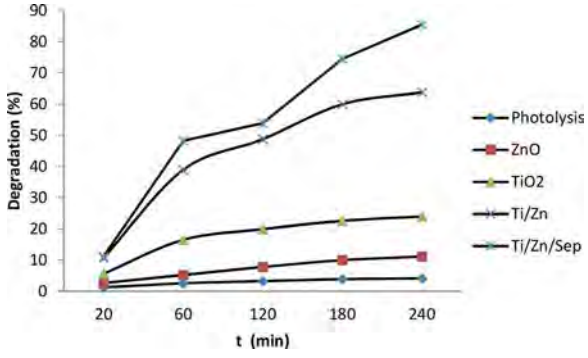

Fig. 7. Photodegradation of FLQ by TiO_2, ZnO, Ti/Zn, and Ti/Zn/Sep catalysts.

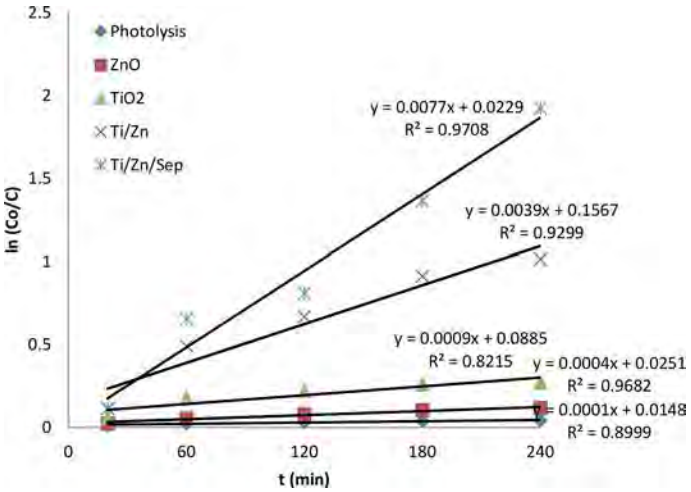

Fig. 8. Plots of ln $\left(\frac{C_o}{C}\right)$ versus irradiation time (t).

composite form and higher surface area. The maximum degradation efficiency was obtained with 85% using Ti/Zn/Sep catalyst within 240 min (Figure 7). This can be attributed to the anatase (89%) form of TiO_2, higher surface area, greater pore size, and greater pore volume which cause rapid diffusion of intermediates during the photocatalytic degradation. These properties have an important way to obtain an efficient photocatalytic reaction. Also the enhanced separation efficiency of charge carriers resulting from the charge transfer between ZnO and TiO_2 caused efficient degradation. The positive effect of ZnO can be explained by extending the adsorption of the radiation in the composite form (Hadjltaief et al., 2016).

From Table I, the k' rate constants are

TiO_2: $k = 9.0 \times 10^{-4}\,\text{min}^{-1}$
ZnO: $k = 4.0 \times 10^{-4}\,\text{min}^{-1}$
Ti/Zn: $k = 39.0 \times 10^{-4}\,\text{min}^{-1}$
Ti/Zn/Sep: $k = 77.0 \times 10^{-4}\,\text{min}^{-1}$

Ti/Zn/Sep catalyst created a dynamic synergy effect in FLQ degradation, with a constant increase in the rate by a factor of 8.5 to pure TiO_2 and 19.5 to pure ZnO. This indicates that the electrons and holes photo-induced from the intercalated ZnO could be much more effectively separated in the photocatalytic degradation of the FLQ (Sun et al., 2002). However, pure ZnO did not show the efficient photocatalytic degradation of the FLQ but it played an important role in the TiO_2/ZnO/Sep system for the degradation of the FLQ. Figure 9 shows the UV-DRS analysis of the TiO_2, ZnO, Ti/Zn, and Ti/Zn/Sep catalysts. It is obvious that all catalysts show strong and quiet similar light absorption profiles in deep UV region.

Table II. Kinetic constants for TiO_2, ZnO, Ti/Zn/Sep

Catalyst	$k \times 10^{-4}$ (min^{-1})	R^2
Ti/Zn/Sep	77	0.97
Ti/Zn	39	0.92
TiO_2	9	0.82
ZnO	4	0.96
Without catalyst (photolysis)	1	0.89

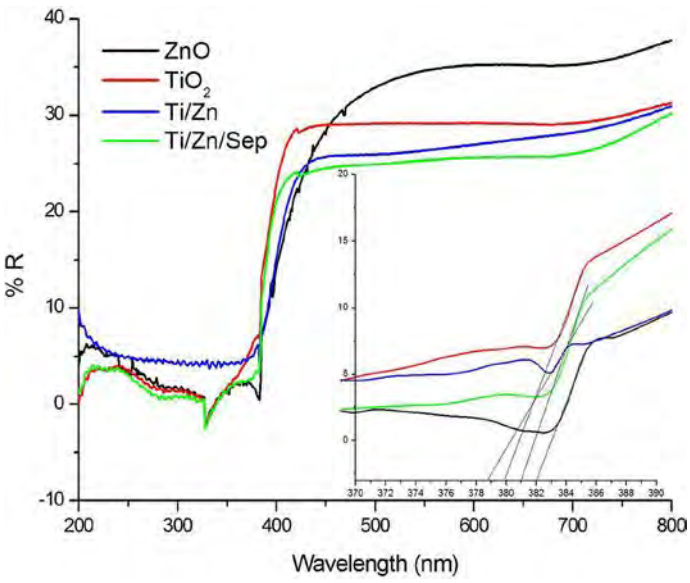

Fig. 9. UV-DRS spectrum of TiO_2, ZnO, Ti/Zn, and Ti/Zn/Sep.

The edges of the band gap of TiO_2, ZnO, Ti/Zn, and Ti/Zn/Sep are 380, 382, 379, and 383 nm, respectively. The band gap energies are 3.26, 3.24, 3.27, and 3.22 eV for TiO_2, ZnO, Ti/Zn, and Ti/Zn/Sep catalysts, respectively (inset in Figure 9), which can be calculated from the onset of the absorption edge (λ_g) using the $E_g = 1240/\lambda_g$ formula. The band gap energy of the Ti/Zn/Sep was slightly lower than that of TiO_2, ZnO, and Ti/Zn. This shift can be explained in two ways. First, the higher quantum confinement from the immobilization of ZnO was led to decrease the band gap energy of the Ti/Zn/Sep catalyst (Reinosa et al., 2016). Second, sepiolite can cause a shift of the absorption edge to a longer wavelength (red shift). These E_g values which are close to each other show that band gap did not play an active role in the FLQ decomposition process. The photocatalytic mechanism of the TiO_2/ZnO composite catalyst is illustrated in Figure 10. The E_{CB} and E_{VB} values of the two semiconductors help to explain the photo-excited charge carriers in the composite form. The E_{CB} and E_{VB} values of TiO_2 and ZnO can be calculated using the following empirical formula (Saravanan et al., 2014):

$$E_{CB} = X - E_e - 0.5E_g$$

$$E_{VB} = X - E_e + 0.5E_g$$

where E_{VB} and E_{CB} are the valance band and conduction band edge potentials, respectively. E_g is the band gap energy of the catalysts. X' represents the electronegativity of the TiO_2 ($X = 5.82$) and the ZnO ($X = 5.79$). E_e is the energy of free electrons on the hydrogen scale (~4.5 eV). The calculated E_{CB} and E_{VB} values of TiO_2 were -0.31 and 2.95 eV and of the ZnO were -0.34 and 2.91 eV, respectively. According to this, when TiO_2 and ZnO absorbed the UV light, the E_{VB} electrons of the ZnO were excited to own E_{CB} where the excited electrons were then transferred to the conduction band of the TiO_2. The trapping of electrons on the E_{CB} of the TiO_2 hindered the recombination of the e^-/h^+ pairs of ZnO which caused enhanced photoactivity. The calculated valence band values for TiO_2 are

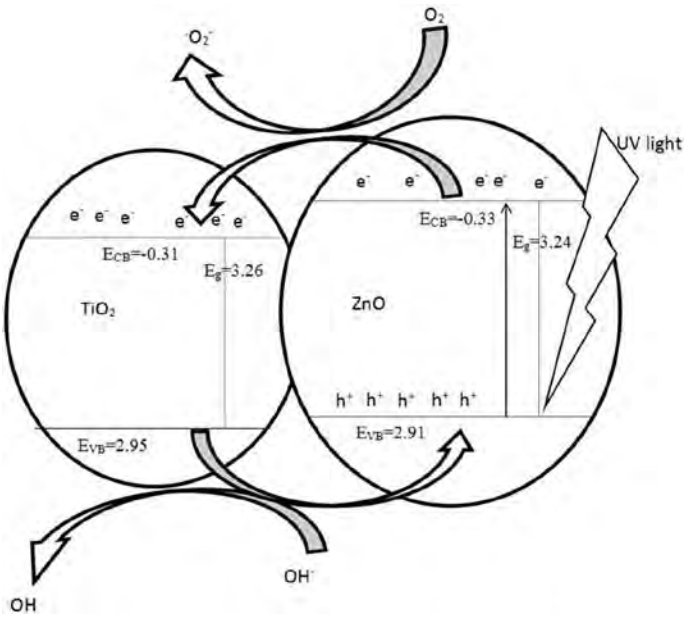

Fig. 10. Charge transfer pathway of catalytic reaction using TiO_2/ZnO/Sep composites under UV light.

greater than ZnO. Therefore, photo-generated holes did not transfer to the valence band of the ZnO.

A series of scavengers experiment has been performed to further explain the photocatalytic mechanism of Ti/Zn/Sep catalyst. Regulska and coworkers suggested that in the photocatalytic degradation process, superoxide ($O_2^{\bullet -}$), hydroxyl ($OH^{\bullet}$), and hole (h^+) radicals play an important role in the degradation of the organic molecules. Hydroxyl radicals attack the benzene ring of higher electron density, and superoxide radicals attack the lower electron density of the pyridine ring (Regulska et al., 2016). In this section, some oxidative ($OH^{\bullet}$, h^+, and $O_2^{\bullet -}$ species) scavengers such as IPA, KI, and AA were used to remove these reactive species (Gan et al., 2013; Lu et al., 2015) (Figure 11). IPA, KI, and AA are $OH^{\bullet}$, h^+, and $O_2^{\bullet -}$ scavengers, respectively. The photocatalytic degradation of FLQ without the addition of any scavengers

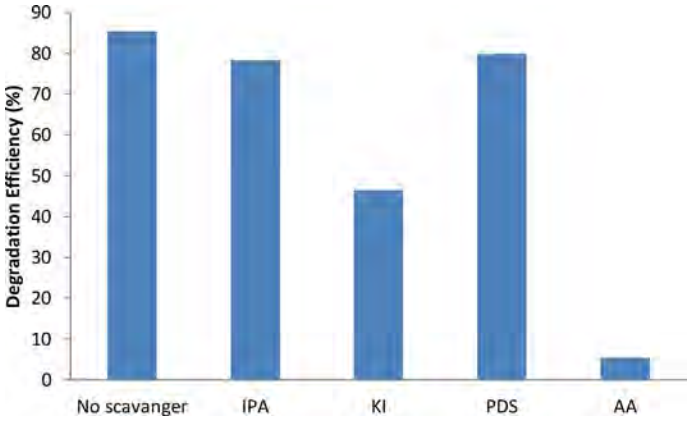

Fig. 11. Effects of different scavengers on degradation of FLQ in the presence of TiO_2/ZnO/Sep composite photocatalyst.

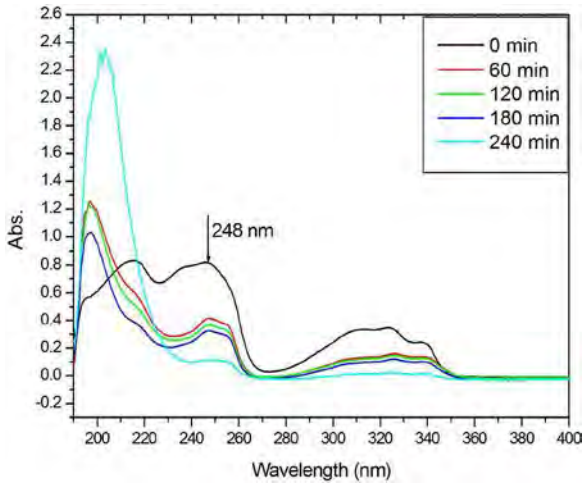

Fig. 12. Evaluation of UV–vis spectra studied at different times of photocatalytic reaction.

reached 85% by Ti/Zn/Sep. In the presence of KI/catalyst system, degradation efficiency mainly decreased to 45.5% indicating that holes (h^+) are the major reactive species on FLQ degradation. However, after adding IPA, the activity of Ti/Zn/Sep did not largely change on FLQ degradation (78.4%). When AA was used as a superoxide scavenger, the catalytic activity of Ti/Zn/Sep was largely decreased, and only 5.5% degradation percentage was obtained within 240 min. These results show that h^+ and $O_2^{\bullet -}$ reactive species could play a major role in the photocatalytic degradation of FLQ using Ti/Zn/Sep.

To reveal degradation efficiency and intermediates, UV–vis and HRMS analysis were performed on FLQ degradation. Figure 12 shows the UV–vis absorption spectra of the FLQ samples at different degradation times. The initial FLQ solution shows two absorption peaks, and the most prominent peak has been seen at 248 nm (Table III). It can be clearly seen that the intensity of the absorption peaks decrease gradually time dependently and almost disappear within 240 min. This implies that FLQ antibiotic was largely degraded within 240 min. In order to support this result, HRMS results have been evaluated. From Figure 13(a), the primary fragment ions are 244 and 226 *m/z* values which respond to the loss of water from protonated molecular ions. The *m/z* at 222 and 224 ions shows loss of C_3H_6 (Figure 13(a)). The fragment ion is provided in Figure 13(b) (*m/z* 179.0952) and individually corresponds losing of CO and

Table III. Chemical data of FLQ

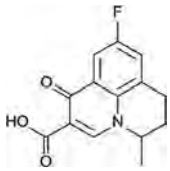

Name: Flumequine
Formula: $C_{13}H_{11}FNOCO_2H$ (it contains carbonyl and carboxyl groups)
Molecular mass: 261.25 g/mol
λ_{max}: 248 nm

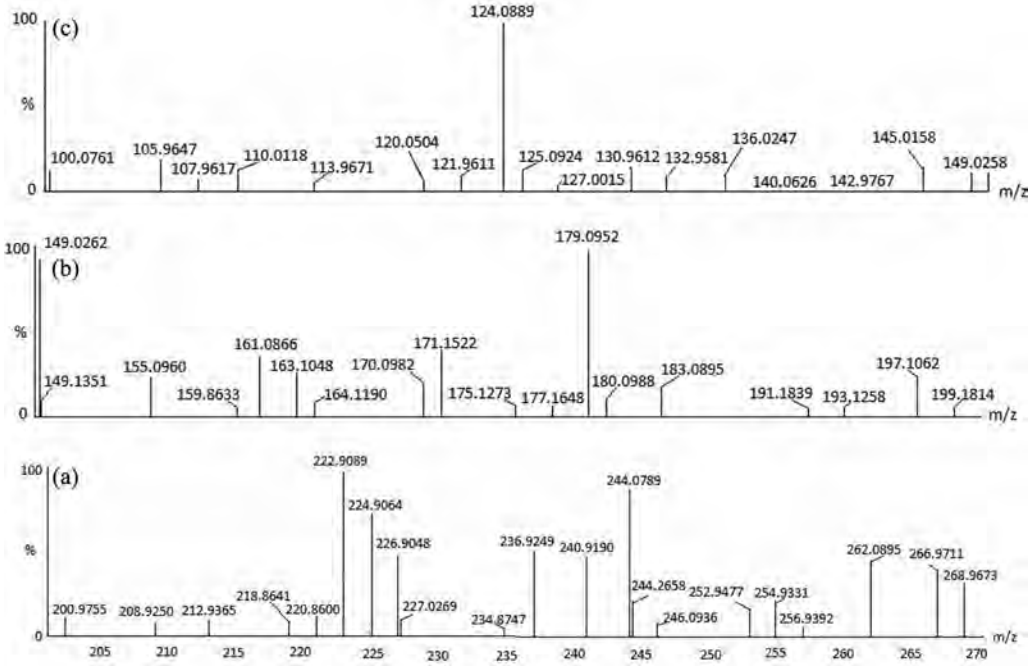

Fig. 13. HRMS analyses at different degradation times (a) 60, (b) 120, (c) 240.

H_2O (from *m*/*z* 222). In Figure 13(c), as shown, the main fragment ion is *m*/*z* 124.0889, implying losses of CO. This observational study suggests that Ti/Zn/Sep catalyst is an efficient material for decomposing organic molecules which have high molecular weight.

Conclusion

The present study shows the enhancement of physiochemical properties and catalytic activity of Ti/Zn/Sep for decomposition of FLQ. The surface of sepiolite was improved by TiO_2 and ZnO insertion in sepiolite structure. The experimental results showed that Ti/Zn/Sep catalyst is more photoactive than Ti/Zn, TiO_2, and ZnO catalysts. The increased adsorption ability for Ti/Zn/Sep supported to enhance the efficiency of the catalytic reaction. ZnO played a primary role by inhibiting the recombination of the electron (e^-) and hole (h^+) pairs.

Funding

This work was supported by the This study was carried out with the support of Mugla Sitki Kocman University, the coordination of scientific research (number 15/139).

References

Abollino, O., Giacomino, A., Malandrino, M., and Mentasti, E. (2008). Interaction of metal ions with montmorillonite and vermiculite, *Appl. Clay Sci.*, **38**, 227–236.

Bhattacharyya, K. G., and Gupta, S. S. (2008). Adsorption of a few heavy metals on natural and modified kaolinite and montmorillonite: A review, *Adv. Colloid Interf. Sci.*, **140**, 114–131.

Chen, M., and Chu, W. (2012). Degradation of antibiotic norfloxacin in aqueous solution by visible-light-mediated C-TiO_2 photocatalysis, *J. Hazard. Mater.*, **219–220**, 183–189.

Elmolla, E. S., and Chaudhuri, M. (2010). Photocatalytic degradation of amoxicillin, ampicillin and cloxacillin antibiotics in aqueous solution using UV/TiO_2 and UV/H_2O_2/TiO_2 photocatalysis, *Desalination.*, **252**, 46–52.

Eydivand, S, and Nikazar, M. (2015). Degradation of 1,2-Dichloroethane in Simulated Wastewater Solution: A Comprehensive Study By Photocatalysis Using TiO_2 and ZnO Nanoparticles, *Chem. Eng. Commun.*, **202**, 102–111.

Gnanaprakasam, A., Sivakumar, V. M., Sivayogavalli, P. L., and Thirumarimurugan, M. (2015). Characterization of TiO_2 and ZnO nanoparticle sand their applications in photocatalytic degradation of azo dyes, *Ecotox. Environ. Safe.*, **121**, 121–125.

Gan, H., Zhang, G., and Huang, H. (2013). Enhanced visible-light-driven photocatalytic inactivation of Escherichia coli by $Bi_2O_2CO_3$/Bi_3NbO_7 composites, *J. Hazard. Mater.*, **250–251**, 131–137.

Hadjltaief, H. B., Zina, M. B., Galvez, M. E., and Costa, P. D. (2016). Photocatalytic degradation of methyl green dye in aqueous solution over natural clay-supported ZnO–TiO_2 catalysts, *J. Photochem. Photobiol. A: Chem.*, **315**, 25–33.

Lu, D., Zhang, G., and Wan, Z. (2015). Visible-light-driven g-C_3N_4/Ti^{3+}-TiO_2 photocatalyst co-exposed {0 0 1} and {1 0 1} facets and its enhanced photocatalytic activities for organic pollutant degradation and Cr(VI) reduction, *Appl. Surf. Sci.*, **358**, 223–230.

Li, H., Zhang, W., Guan, L., Li, F., and Yao, M. (2015). Visible light active TiO2–ZnO composite films by cerium and fluorine codoping for photocatalytic decontamination, *Mater. Sci. Semicond. Proc.*, **40**, 310–318.

Mahdavi, S., Jalali, M., and Afkhami, A. (2013). Heavy metals removal from aqueous solutions using TiO_2, MgO, and Al_2O_3 nanoparticles, *Chem. Eng. Comm.*, **200**, 448–470.

Madejov, J., and Komadel, P. (2001). Baseline studies of the clay minerals society source clays: ınfrared methods, *Clays CIay Miner.*, **49**, 410–432.

Nikolaou, A., Meric, S., and Fatta, D. (2007). Occurrence patterns of pharmaceuticals in water and wastewater environments, *Anal. Bioanal. Chem.*, **387**, 225–1234.

Palominos, R., Freer, J., Mondaca, M. A., and Mansilla, H. D. (2008). Evidence for hole participation during the photocatalytic oxidation of the antibiotic flumequine, *J. Photochem. Photobiol. A: Chem.*, **193**, 139–145.

Robert, D., and Malato, S. (2002). Solar photocatalysis: a clean process for water detoxification, *Sci. Total Environ.*, **291**, 85–97.

Rodrigues-Silva, C., Maniero, M. G., Rath, S., and Guimarães, J. R. (2013). Degradation of flumequine by photocatalysis and evaluation of antimicrobial activity, *Chem. Eng. J.*, **224**, 46–52.

Reinosa, J. J., et al. (2016). Enhancement of UV absorption behavior in ZnO–TiO_2 composites, *Bol. Soc. Esp. Cerám. Vidr.*, **55**, 55–62.

Regulska, E., Brus, D. M., Rodziewicz, P., Sawicka, S., and Karpinska, J. (2016). Photocatalytic degradation of hazardous Food Yellow 13 in TiO_2 and ZnO aqueous and river water suspensions, *Catal. Today.*, **266**, 72–81.

Saravanan, R., Gupta, V. K., Mosquera, E., and Gracia, F. (2014). Preparation and characterization of V_2O_5/ZnO nanocomposite system for photocatalytic application, *J. Mol. Liq.*, **198**, 409–412.

Singh, A., Kumar, R., Malhotra, N., and Suman, M. (2012). Preparation of ZnO nanoparticles by solvothermal process, *Int. J. Sci. Emer.*, **4**(1), 49–53.

Sun, Z., Chen, Y., Ke, Q., Yang, Y., and Yuan, J. (2002). Photocatalytic degradation of cationic azo dye by TiO_2/bentonite nanocomposite, *J. Photochem. Photobiol. A.*, **149**, 169–174.

Uğurlu, M., and Karaoğlu, M. H. (2011). TiO_2 supported on sepiolite: Preparation, structural and thermal characterization and catalytic behavior in photocatalytic treatment of phenol and lignin from olive mill wastewater, *Chem. Eng. J.*, **166**, 859–867.

Wang, H., Li, J., Chang, M., Guana, Q., Lu, Z., Huo, P., and Yan, Y. (2015). Melamine modified P25 with heating method and enhanced the photocatalytic activity on degradation of ciprofloxacin, *Appl. Surf. Sci.*, **329**, 17–22.

Wang, Y., Zhu, S., Chen, X., Tang, Y. Y., Peng, J. Z., and Wang, H. (2014). One-step template-free fabrication of mesoporous ZnO/TiO_2 hollow microspheres with enhanced photocatalytic activity, *Appl. Surf. Sci.*, **307**, 263–271.

Xu, WG., Liu, S. F., Lu, S. X., Kang, S. Y., Zhou, Y., and Zhang, H. F. (2010). Photocatalytic degradation in aqueous solution using quantum-sized ZnO particles supported on sepiolite, *J. Colloid Interf. Sci.*, **351**, 210–216.

Ye, J., Li, X., Hong, J., Chen, J., and Fan, Q. (2015). Photocatalytic degradation of phenol over ZnO nanosheets immobilized on montmorillonite, *Mater. Sci. Semicond. Proc.*, **39**, 17–22.

Zhou, W., Liu, K., and Fu, H. (2008). Multi-modal mesoporous TiO_2– ZrO_2 composites with high photocatalytic activity and hydrophilicity, *Nanotechnology*, **19**, 035610–035616.

Zhu, C., Wang, L., Kong, L., Yang, X., Wang, L., Zheng, S., Chen, F., MaiZhi, F., and Zong, H. (2000). Photocatalytic degradation of Azo dyes by supported (TiO_2 + UV) in aqueous solution, *Chemosphere*, **41**, 303–309.